Investigation on the strategies for discharge capacity improvement of aprotic Li-CO_2 batteries

Xu Xiao[a], Wentao Yu[a], Wenxu Shang[a], Peng Tan[a*], Yawen Dai[b], Chun Cheng[b], Meng Ni[b,c*]

[a.] Department of Thermal Science and Energy Engineering, University of Science and Technology of China, Hefei 230026, Anhui, China.
[b.] Department of Building and Real Estate, The Hong Kong Polytechnic University, Hung Hom, Kowloon, Hong Kong, China.
[c.] Environmental Energy Research Group, Research Institute for Sustainable Urban Development (RISUD), The Hong Kong Polytechnic University, Hung Hom, Kowloon, Hong Kong, China.

*Corresponding authors:
Email: pengtan@ustc.edu.cn (Peng Tan)
Email: meng.ni@polyu.edu.hk (Meng Ni)

Abstract: Aprotic Li-CO_2 batteries offer a sustainable strategy for large-scale CO_2 fixation and meanwhile providing electricity with high specific energy densities. However, the limited practical capacity hinders the application of this technology. To achieve a high-capacity Li-CO_2 battery, parameter sensitivity analysis based on a developed model is conducted in this work to identify the limiting factors. It is found that the initial porosity of the cathode is the most determining factor to the specific capacity. To this end, various cathode structures including hierarchical, tapered, parabolic, trapezoid, and frustum conical pore distribution modes are designed and evaluated. Among these designs, the frustum conical porous cathode can lead to the largest capacity improvement of over 60%, demonstrating the feasibility of improving the capacity through structure design. Besides, the present sensitivity analysis system is evaluated at high current densities, and the experimental approaches for fabricating

the designed cathodes are proposed and detailly elaborated. This work highlights the effective cathode structure design for high-performance aprotic Li-CO_2 batteries.

Keywords: Aprotic Li-CO_2 battery; Discharge capacity; Parameter sensitivity analysis; Pore distribution; Structure design

1. Introduction

Metal-CO_2 batteries, which integrate CO_2 fixation with energy conversion, provide promising strategies to relieve the shortage of fossil fuels and broaden the field of sustainable energy [1,2]. Besides, realizing the potential impact of CO_2 is favorable to develop actual metal-air batteries on the condition of ambient air (i.e. O_2, CO_2, and H_2O) [3,4]. The battery operation is the direct absorption and release of the fuel CO_2 during discharge and charge, respectively, exploiting excellent application prospects in the field of submarines mission and even Mars exploration at a high CO_2 atmosphere (~96%) [5,6]. To this end, multitudes of scientific efforts have been made to overcome technical barriers and promoting electrochemical performance, from the aspects of understanding the reaction mechanisms [7,8], designing the available catalysts [9,10], stabilizing the electrolyte compositions [11,12], protecting the mental anodes [13,14], modifying the operation conditions [15,16], and improving the electrode structures [17,18].

Among various metal-CO_2 batteries, aprotic Li-CO_2 batteries have attracted broader attention because of the high equilibrium potential of 2.8 V and theoretical energy density of 1876 Wh kg^{-1}. Since the primary Li-CO_2 battery as a new energy

storage technology was proposed first by Archer et al. [19], research mainly focuses on elevating the discharge capacity, rate capability, and cycling stability of the complex electrochemical/chemical system [20–22]. Afterward, Zhou et al. showed that by designing a carbon nanotubes (CNTs) cathode and a tetraglyme (TEGDME)-based electrolyte, a Li-CO_2 battery could deliver a large specific capacity of 8379 mAh g^{-1} and a stabilized cycle life of 29 times at 50 mA g^{-1} at room temperature [23]. Ni nanocatalyst decorated on N-doped graphene (Ni-NG) was also applied to improve rate capability and cyclability, which harvested a longer lifespan of over 100 cycles with a fixed 1000 mAh g^{-1} capacity per cycle at 100 mA g^{-1} [24]. Inspired by a plant absorbing CO_2 for photosynthesis, Hu et al. fabricated a flexible wood coated with a Ru-loaded CNT network, which could not only provide transport channels for gas and liquid inside the wood structure but also support electron transfer across the exterior carbon network [17]. Consequently, stable cycling for more than 200 times with a reduced overpotential of 1.5V was achieved at 200 mA g^{-1}. Similarly, a nitrogen-doped double-layered three-dimensional carbon nanotube/graphene (3D NCNT/G) cathode led to a high discharge capacity of 17534.1 mAh g^{-1} with high coulombic efficiency of 98.3% at 100 mA g^{-1} [18]. Apart from the aprotic electrolytes (i.e. ether or sulfone), liquid-free electrolytes have been successfully developed to assist the operating stability. A polymer-based Li–CO_2 battery with a binuclear cobalt phthalocyanine-containing gel polymer electrolyte (Bi-CoPc-GPE) exhibited an ultra-large capacity of 27196 mAh g^{-1} and superior cycling ability of up to 120 times

without performance decay [25]. Further, a composite anode made of a carbon film deposited on metal Li was adopted to inhibit dendrites generation and keep electrochemical stability of 115 cycles with a cut-off capacity of 500 mAh g^{-1}, which presented three times better durability than the battery with the pristine Li metal [14]. In addition to battery materials, the operating conditions were also explored, such as the current density, CO_2 partial pressure, and working temperature. For example, at an ultra-low temperature of -60 ℃, a Li-CO_2 battery unexpectedly obtained a superior full discharge capacity to 8976 mAh g^{-1} and cycling performance of over 150 cycles (1500 h) at 100 mA g^{-1} [16]. The current density was demonstrated to play an important role in modifying the formation and decomposition of Li_2CO_3 and C, in which a small current density induces small particles of crystalline Li_2CO_3 while a large current density causes large particles of Li_2CO_3 crystals and decreases the charge voltage [15].

Even with great progress in Li-CO_2 batteries, it is still difficult to experimentally analyze the influence of individual parameters on the electrochemical performance. In comparison, modeling and simulation with an intensive understanding of the reaction mechanisms are expected to address experimental limitations and investigate the electrochemical characteristics of the battery. Up to now, simulations on aprotic Li-O_2 batteries have provided useful guidance for experiments. For example, Liu et al. assumed a hierarchical cathode structure and investigated the effect of different porosity span on discharge voltage curves [26,27]. Franco et al. evaluated a bi-porous

cathode with mesopores and macropores and further instructed the experiments of the porous structure in the carbon black and Co-doped NiO electrodes [28–30]. Li et al. assessed the cathode wettability with various electrolyte saturations and revealed the significance of the suitable gas-liquid two-phase interface inside the porous electrode [31–33]. However, such modeling works and numerical investigations are extremely rare in Li-CO_2 batteries.

In our previous work, a multiphysics-coupled Li-CO_2 battery model in the continuum scale is developed, and the numerical results indicate the substantial different behaviors compared to the aprotic Li-O_2 batteries owing to the different fundamental reaction mechanisms and transport properties [15]. Thus, performing numerical analysis of Li-CO_2 batteries to examine the effects of different parameters is necessary for identifying the limiting factors and improving the electrochemical performance. Herein, we first conducted the parameter sensitivity analysis based on the previous model to figure out the key parameter to the specific discharge capacity. Subsequently, various design cases were proposed and simulated to evaluate their effectiveness for maximizing the discharge capacity. Further, the sensitivity analysis limitations at high rate capability were discussed, and the experimental methods for the implementation of the optimal design were proposed. This work is favorable to systematical investigation and effective optimization of the discharge performance of aprotic Li-CO_2 batteries.

2. Model development

An aprotic Li-CO_2 battery is schematically shown in **Fig. 1**. The electrochemical reactions during discharge occur at metal anode and porous cathode are as follows:

Anode: $Li \rightarrow Li^+ + e^-$ (E^0=0 V vs. Li^+/Li) (I)

Cathode: $4Li^+ + 4e^- + 3CO_2 \rightarrow 2Li_2CO_3 + C$ (E^0=2.80V vs. Li^+/Li) (II)

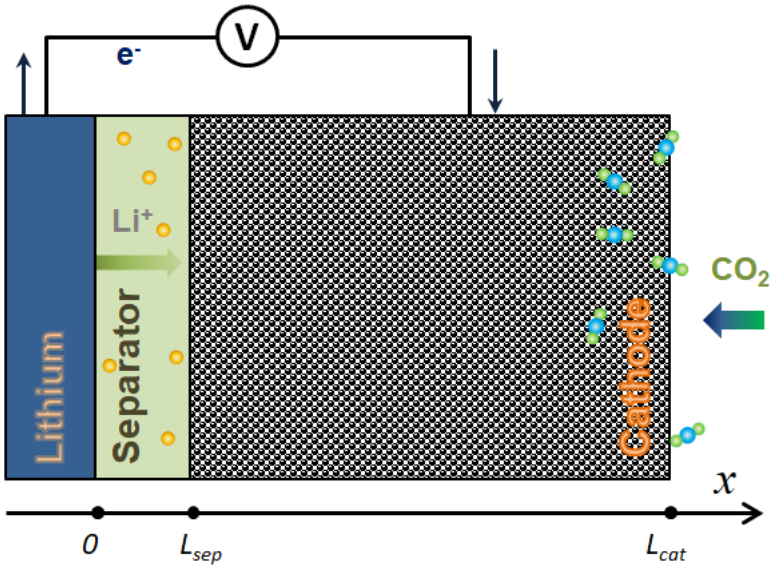

Fig. 1. Scheme of the discharge process of an aprotic Li-CO_2 battery with a lithium metal anode, separator, and a porous cathode.

2.1 Basic governing equations

A one-dimensional model was developed to describe the mass transport, electrochemical reaction, and passivation mechanisms in a Li-CO_2 battery, as reported in our previous work [15]. The fundamental equations include the species transport of Li^+ and CO_2 in the electrolyte as:

$$\frac{\partial(\varepsilon_l c_j)}{\partial t} = -\nabla \cdot N_j + R_j \quad (1)$$

where ε_l is the porosity of the cathode, c_j is the bulk concentration of species j in the

electrolyte (mol m^{-3}). N_j is the molar flux of species j due to the diffusion and migration, and R_j is the reaction rate of species j, which is coupled to the electrochemical kinetics in the anode and cathode as:

$$I_{\mathrm{a}} = Fk_{\mathrm{Li}}c_{\mathrm{Li}}^{\alpha}\left\{\exp\left[\frac{(1-\alpha)F}{RT}\eta\right]-\exp\left(\frac{-\alpha F}{RT}\eta\right)\right\} \quad (2a)$$

$$I_{\mathrm{c}} = F\left\{k_{\mathrm{a}}(c_{\mathrm{Li_2CO_3}}^{2})(c_{\mathrm{C}})\exp\left[\frac{(1-\alpha)F}{RT}\eta\right]-k_{\mathrm{c}}(c_{\mathrm{Li}}^{4})(c_{\mathrm{CO_2}}^{3})\exp\left(\frac{-\alpha F}{RT}\eta\right)\right\} \quad (2b)$$

where I is interfacial current density (mA cm^{-2}), k_{Li}, k_{a}, and k_{c} are lithium, anodic and cathodic rate constants, respectively, α is the symmetry factor (0.5), F is Faraday constant, R is the ideal gas constant, T is the temperature (K), and η is the overpotential that is associated with the electrode potential (ϕ_{s}) and electrolyte potential (ϕ_{l}) as:

$$\eta = \phi_{\mathrm{s}} - \phi_{\mathrm{l}} - E_{eq} - \Delta\phi_{s,\,film} \quad (3)$$

where E_{eq} is the equilibrium potential, $\Delta\phi_{s,\,film}$ is the potential drop that dynamically changes with the solid insulated product of Li_2CO_3 and C on the electrode surface as:

$$\varepsilon_{s,\,film} = \sum\left(\frac{c_{Li_2CO_3}}{\rho_{Li_2CO_3}/W_{Li_2CO_3}}+\frac{c_C}{\rho_C/W_C}\right) \quad (4)$$

where $\varepsilon_{s,\,film}$ represents the product volume fraction, W and ρ are the molecular weight (g mol^{-1}) and the density (kg m^{-3}). The detailed governing equations are listed in **Supporting Information**.

2.2 Parameter sensitivity analysis

When changing the value of different parameters (e.g., porosity, electrode thickness) in the model, the effects on the specific discharge capacities of the battery

are different. Thus, a parameter sensitivity analysis is necessary to investigate the effect on the discharge capacity and elucidate the capacity-limiting factors. The parameter sensitivity index M_i at the applied current density i is conducted as [34]:

$$M_i = \sqrt{\frac{1}{k}\sum_{n=1}^{k}\left[\frac{G_i(x_n)}{X_n}\right]^2} \tag{5}$$

where $G_i(x)$ is the change ratio of the specific capacity when the analysis value of the parameter is x, and X_n is the change ratio of the analysis value of the parameter, which are computed as:

$$G_i(x_n) = \frac{g_i(x_n) - g_i(x_0)}{g_i(x_0)} \tag{6}$$

$$X_n = \frac{x_n - x_0}{x_0} \tag{7}$$

where x_0 is the initial parameter value, x_n is the analysis value of parameter selected from variation range *n*, $g_i(x)$ is the specific capacity when the parameter value is x, and *k* is the number of selective analysis values equally spaced within the parameter variation range.

2.3 Numerical conditions

The initial parameter values and applied current densities are based on the experiments using carbon nanotubes (CNTs) as the cathode material conducted at pure CO_2 with the pressure of 1 atm, as listed in **Table 1**. For solving the discharge process, a finite element method based on the COMSOL platform is used by setting the maximum time step of 0.1 s and relative tolerance of 10^{-4}.

As shown in **Fig. 2**, the discharge voltage curves calculated by our model fit well with experimental data, demonstrating the validity of the model for further analysis. The ranges of all parameters for sensitivity analysis are also listed in **Table 1**, and the analyzed values are equally spaced in the variation ranges (e.g., the thickness of the separator is set as 25, 37.5, 50, 62.5, and 75). The parameter sensitivity analysis is conducted on the constant-current discharge mode with different current densities (i_{app} = 0.05, 0.1, 0.2, 0.3, 0.4, and 0.5 mA cm^{-2}).

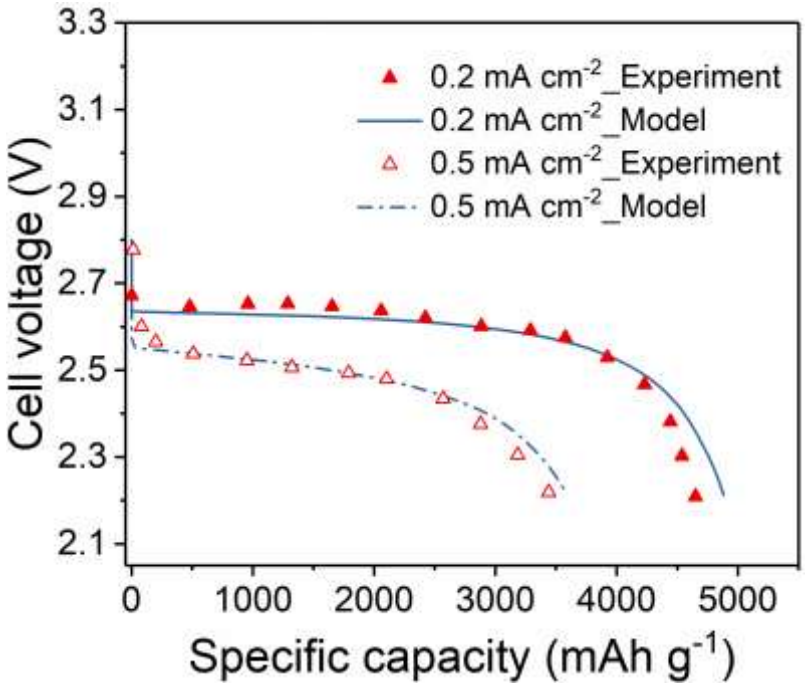

Fig. 2. The comparison between the simulated voltage curves and the experimental data with a cut-off voltage of 2.2 V [20,35].

Table 1 Lists of parameters used in the calculation

Parameter	Symbol	Initial value x_0	Ref.	Variation range x_n	Sensitivity Index M_{avg}	Parameter Categories
Thickness of the separator	L_{sep}	50 μm	[36]	25～75	4.47 × 10^{-3}	Insensitive

Thickness of the porous cathode	L_{cat}	500 μm		200～750	1.82×10^{-1}	Sensitive
Porosity of the separator	ε_{sep}	0.87	[37]	0.84～0.90	1.56×10^{-2}	Sensitive
Porosity of the cathode	$\varepsilon_{l,0}$	0.907		0.877～0.937	1.28×10^{1}	Very Sensitive
Conductivity of the cathode	σ	30 S m^{-1}	[38]	15～30	1.61×10^{-3}	Insensitive
Carbon nanotube radius	r_0	20 nm	[39]	10～30	2.58×10^{-1}	Sensitive
The volume percentage of the solid Li_2CO_3 in the total product	φ	92.95%	[40]	92.75%～92.95%	7.24×10^{-1}	Very Sensitive
Initial Li^+ concentration	c_{Li}	1 M	[20]	0.9～1.1	1.51×10^{-2}	Sensitive
Initial CO_2 concentration	c_{CO_2}	0.12 M	[41]	0.1～0.14	2.23×10^{-1}	Sensitive
Diffusion coefficient of Li^+	D_{Li}	8.98×10^{-10} m^2 s^{-1}	[42]	4.49×10^{-10}～1.35×10^{-9}	2.69×10^{-3}	Insensitive
Diffusion coefficient of CO_2	D_{CO_2}	2.32×10^{-10} m^2 s^{-1}	[43]	1.16×10^{-10}～3.48×10^{-10}	3.21×10^{-1}	Sensitive
Conductivity of the electrolyte	κ	0.03 S m^{-1}	[42]	0.024～0.036	1.38×10^{-1}	Sensitive
Reaction rate coefficient of anodic current	k_a^*	1.11×10^{-14} m^4 mol^{-1} s^{-1}	Assumed	1.11×10^{-15}～1.11×10^{-13}	4.36×10^{-3}	Insensitive
Reaction rate coefficient of cathodic current	k_c^*	2.38×10^{-32} m^{19} mol^{-6} s^{-1}	Assumed	2.38×10^{-32}～2.38×10^{-30}	2.46×10^{-1}	Sensitive
Reaction rate coefficient of Li metal	k_{Li}^*	10^{-5} m s^{-1}	Assumed	10^{-6}～10^{-4}	1.39×10^{-1}	Sensitive
Electrical resistivity of hybrid product	R_s	10^{10} Ω m	Assumed	0.9×10^{10}～1.1×10^{10}	6.53×10^{-2}	Sensitive

* Sensitivity analysis of the reaction rate coefficients (e.g., k_a, k_c, and k_{Li}) is calculated by a logarithmic pattern.

3. Results

3.1 Effects of various parameters on the discharge performance

Among reported Li-CO_2 batteries, carbon materials with different morphologies have been used in cathodes, which can be generally classified into carbon powder, nanotube, and sheet based on the geometry (**Fig. S1**). As demonstrated in **Fig. S2**, the discharge voltage curves are varied using different carbon materials according to the conversion of the shape factor. Specifically, the calculated capacity using CNTs (3590 mAh g^{-1}) is much higher than that using graphene (2692 mAh g^{-1}) but a little lower than that using KB (3820 mAh g^{-1}) at a high rate of 0.5 mA cm^{-2}, which is caused by the utilization of the void space of the three-dimensional structure by solid Li_2CO_3 and C. Here, the CNT-based cathode is used as a representative in the present study, and other carbon materials can be analyzed using the similar method.

The sensitivity index of 16 major parameters at 6 current densities is displayed in **Fig. 3**. The discharge capacity, regardless of the battery composition, is always varying at different current densities [10,44,45], and the sensitivity index of major parameters is inevitably affected by the applied current density but always maintains the same order of magnitude. The sensitivity index for most parameters increases with an increase of the current density, suggesting that these parameters are linked more closely to the capacity at a high current density. Besides, the sensitivity index for some parameters either fluctuates or decreases with an increase of the current density. Thus, the average sensitivity index at different current densities is conducive to weigh

the extent of the parameter on the discharge capacity. It is found that the sensitivity index is significantly different for different parameters. For example, the sensitivity index of cathode porosity is over 12.46 but becomes only 0.012 for the anodic rate coefficient. To demonstrate the influences, three categories are introduced to classify parameters, referring to insensitive (M_{avg} < 0.01), sensitive (0.01 < M_{avg} < 0.5), and very sensitive (M_{avg} > 0.5), as presented in **Table 1**.

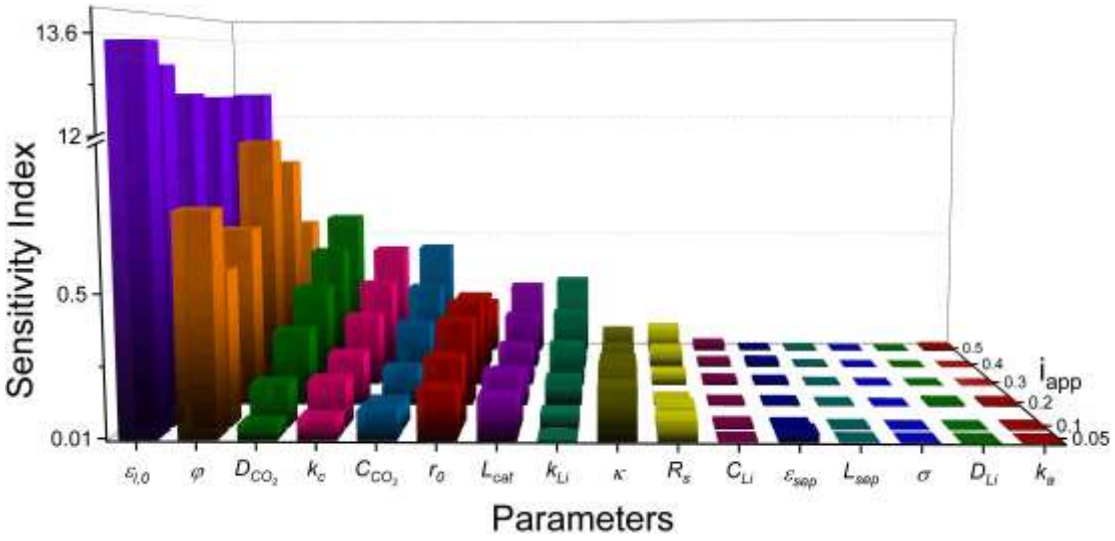

Fig. 3. The sensitivity index of 16 major parameters calculated at 6 current densities (mA cm^{-2}).

Clearly, several parameters can greatly influence the specific capacity, such as the cathode porosity ($\varepsilon_{l,0}$), cathode thickness (L_{cat}), cathodic rate coefficient (k_c), the CNT radius (r_0), solubility (c_{CO_2}) and diffusion (D_{CO_2}) of CO_2, conductivity of the electrolyte (κ), Li_2CO_3 volume ratio in the total product (φ), and product resistivity (R_s). This result is consistent with the research hotspots of Li-CO_2 batteries, demonstrating that the feasible strategies for capacity improvement are carried out on the cathode design, the catalyst availability, and the electrolyte compatibility [25,46].

Superior to the average sensitivity of all analyzed parameters, the most sensitive parameter is found to be the cathode porosity with the highest sensitivity of 12.8, demonstrating that the initial porosity is the most important factor affecting the specific capacity. Therefore, the following work is mainly focused on the cathode structure design characterized by the porosity distribution.

3.2 Cathode structure design

Fig. 4 shows the porosity evolution with the discharge process proceeding under different current densities, and the voltage curves have been validated in **Fig. 2**. To simplify the analysis, the dimensionless distance is defined as $\xi = \left(x - L_{sep}\right) / \left(L_{cat} - L_{sep}\right)$, and its value is located at 0 ~ 1. For the original porosity which is uniform in the cathode (**Fig. 5a**), at the initial discharged stage, the separator side (ξ=0) of the cathode is more likely to capture the insoluble products than the gas side (ξ=1) since CO_2 is saturated in the electrolyte and the separator side has a short Li^+ transport route. With the discharge proceeds, the porosity at the gas side is utilized effectively because of the short CO_2 transport route and the obstruction of the internal transport channel. Eventually, the accumulated products are relatively more near two edges but less in the center of the cathode at the terminal stage.

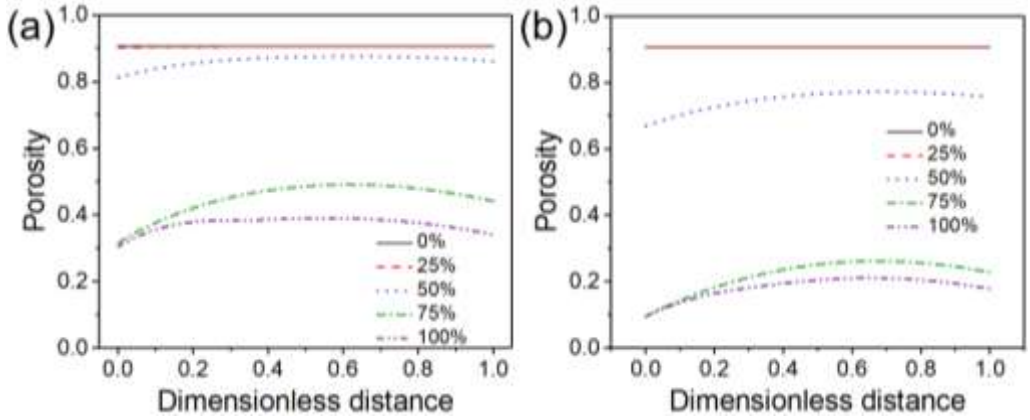

Fig. 4. Porosity evolution in the cathode at different discharge states at the current densities of (a) 0.5 and (b) 0.2 mA cm^{-2}.

From the above study, a uniform porosity leads to the low utilization of the void volume and a low discharge capacity. To this end, a cathode with non-uniform porosity is proposed. Different from previous works in which the gradient porosity is proposed [26,28], the cathode is designed into hierarchical, tapered, parabolic, trapezoid, and frustum conical pore distribution modes in this work, as schemed in **Fig. 5.** Near both sides of the cathode, a large porosity is set to accelerate mass transport and accumulate solid products. In addition, a symmetric structure is applied in all cathode designs owing to the porosity evolution at the end of discharge. In the middle of the cathode, a small porosity is set to enhance the mechanical strength. For quantitative analysis, the porosity distribution is computed by the integration of a given product-filled space:

$$\int_0^1 \varepsilon_{l,0}(\zeta)\, d\zeta \equiv C \tag{8}$$

where $\varepsilon_{l,0}(\zeta)$ is the analyzed porosity when ζ ranges from 0 to 1, and C is the constant value calculated by the uniform porosity in the origin model, and the smallest

initial porosity used in the simulation is set to be 0.9.

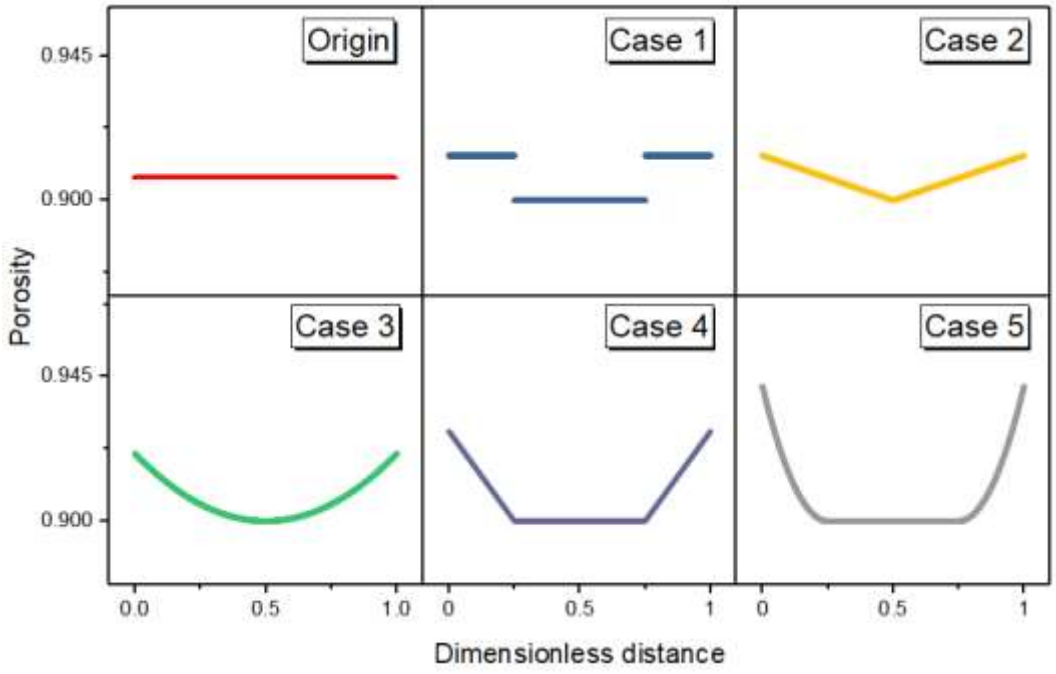

Fig. 5. Different cathode structure: homogeneous (Origin), hierarchical (Case 1), tapered (Case 2), parabolic (Case 3), trapezoid (Case 4), frustum conical (Case 5) porous cathodes.

The five cathode structures are brought into the developed model for simulation, and the effects on the specific capacity and the porosity evolution are illustrated in **Fig. 6**. Under the density currents of 0.5 and 0.2 mA cm^{-2}, the specific capacity and improvement are listed in **Table 2**. In Case 1, a three-layer cathode delivered a capacity increase of over 8%, indicating that using the transition layers is hard to fully utilize the large-porosity space. Then, the concept of continuous gradient porosity is proposed, as shown in Case 2. However, the range of porosity evolution is constricted in spite of the tapered case, leading to a similar increase of about 8%. To smooth the porosity distribution curve, the specific capacities by using a parabolic porosity

distribution (Case 3) seem to achieve the higher level, and the calculated values are 4270.81 and 5789.55 mAh g^{-1} at 0.5 and 0.2 mA cm^{-2}, respectively. Through the above analysis, the cathodes using the trapezoid and frustum conical modes may offer promising potential for capacity enhancement. Inspired by the layered and linear elements, a porous cathode with a trapezoid pore distribution (Case 4) can greatly extend the discharge capacity to 4684.75 and 6360.07 mAh g^{-1} at 0.5 and 0.2 mA cm^{-2}, respectively. Notably, a frustum conical mode (Case 5) provides the largest capacity improvement of more than 60%, suggesting that the combination of the layered and curved techniques is better than both the single and other composite porous cathodes.

Concerning the porosity evolution, the capacity increase at the same density current is determined by the degree of product filling [47]. The span of the terminal porosity becomes more and more narrow as the designed mode upgrading, as shown in **Fig. 6**. In practical applications, the discharge time as a visual indicator to capacity can be easily observed and further evaluated from the experiment apparatus or commercial software [48,49]. The effects of structure designs on the specific capacity are similarly no matter at high or low current densities, suggesting the effectiveness of the proposed designs.

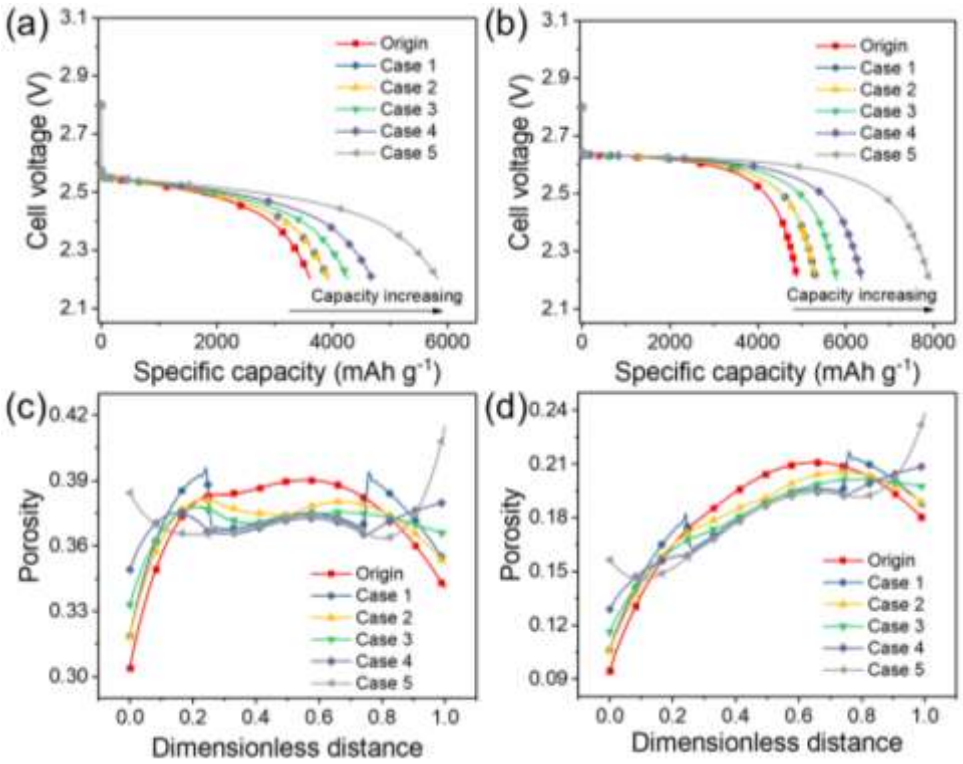

Fig. 6. Discharge performance of different cathode cases: (a-b) discharge voltage curves at the current density of (a) 0.5 and (b) 0.2 mA cm^{-2}; (c-d) porosity evolution at the end of discharge at the current density of (c) 0.5 and (d) 0.2 mA cm^{-2}.

Table 2 Specific capacities and improvement at different cathode structures.

Cathode type	0.5 mA cm^{-2}		0.2 mA cm^{-2}	
	Specific capacity (mAh g^{-1})	Improvement (%)	Specific capacity (mAh g^{-1})	Improvement (%)
Origin	3611.83	-	4881.03	-
Case 1	3923.94	8.64	5317.01	8.93
Case 2	3914.01	8.37	5307.02	8.73
Case 3	4270.81	18.25	5789.55	18.61
Case 4	4684.75	29.71	6360.07	30.30
Case 5	5826.17	61.31	7895.62	61.76

4. Discussion

In the above sections, the key parameter for capacity enhancement is determined through sensitivity analysis, and the electrode structure is optimized. In this section, we will discuss the existing limitation of the present model and the practical fabrication of the designed cathode structure.

4.1 Performance evaluation at high current densities

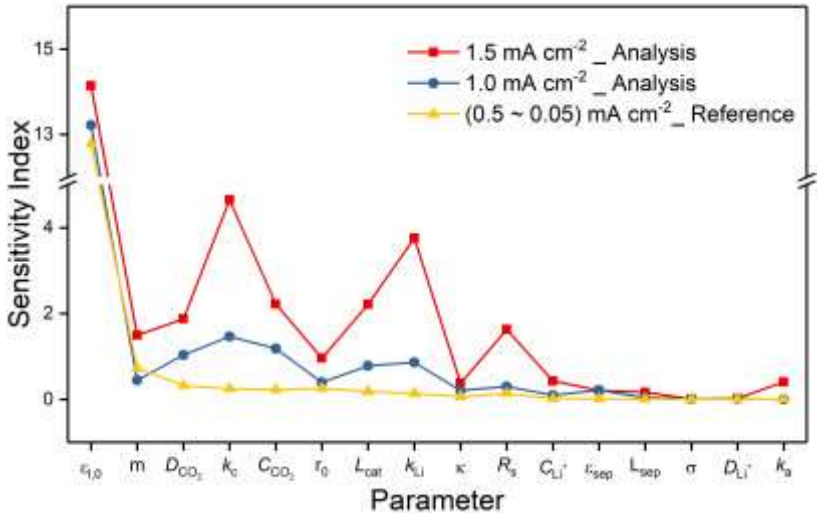

Fig. 7. Sensitivity evaluated at high current densities of 1.0 and 1.5 mA cm^{-2} and compared with the average sensitivity index.

The sensitivity analysis is operated at the high current densities of 1.0 and even 1.5 mA cm^{-2}. As shown in **Fig. 7**, the sensitivity index for several parameters unexpectedly involves several orders of magnitude change, such as cathodic rate coefficient (k_c), Li rate coefficient (k_{Li}), cathode thickness (L_{cat}), solubility (c_{CO_2}) and diffusion (D_{CO_2}) of CO_2. This may be caused by two reasons, including the inferior rate performance in the numerical analysis and the changed product morphology in the model development [23,40]. Firstly, the specific capacity at a high current density

shrinks sharply to 1823.6 and 633.8 mAh g^{-1}, as demonstrated in **Fig. S3**. Consequently, a small change due to the system parameter disturbance can cause a large change ratio. Secondly, the present model neglects the change of product morphology as the discharge current density switches, which is directly evidenced by the observation of CNTs-based cathodes from our experimental studies (**Figs. S1g**, **h**, and **k)** [15]. With an increase of the current density, especially reaching a high value, the product morphology may change significantly (**Fig. S4**). To this end, the morphology effects should be considered for calculating the capacity. Therefore, the sensitivity analysis has limitations in a wide current density range and needs to be improved in combination with the actual capacity and the product morphology.

4.2 Fabrication methods for cathodes with non-uniform porosity

According to the structure design, the frustum conical porous cathode (Case 5) is the best candidate to improve the discharge capacity of Li-CO_2 batteries in this study. To fabricate the cathode with non-uniform porosity distribution, two experimental methods are proposed, as schemed in **Fig. 8**.

The first one is making use of the anodic aluminum oxide (AAO) template-assisted technique [50,51]. The AAO backbone as a substrate has ordered cellular structure with vertically aligned and well-defined open channels (**Fig. 8a**), which can efficiently facilitate the transportation of ions and gas species. Depositing a non-uniform carbon film on the interior walls of an AAO substrate to fabricate the desired cathode with gradient porosity is feasible by the carbonization of the precursor.

The synthesis procedure is as follows: the precursor (e.g., sucrose) is dissolved in distilled water to form a concentrated solution. Then, the homogeneous solution is dripped on the surface of the AAO template for several times, and the volume loading of the precursor is modulated with infiltrated numbers along with the thickness orientation. Subsequently, the AAO template is dried in a vacuum oven and further carbonized under a high-temperature inert-gas atmosphere. Finally, the aimed cathode with a non-uniform porosity is obtained.

The second one is tailoring a hierarchically multiscale porous carbon foam cathode with different porosity distribution based on the silica microspheres (**Fig. 8b**) [52,53]. Specifically, the preparation process includes the following steps: silica spheres with different diameters are assembled layer-by-layer to a vertically stratified structure through vacuum filtration. Then, the precursor solution is fully saturated the framework. After drying in vacuum and further carbonized, the silica template is removed through alkaline solutions. The silica templates can also be other materials such as polystyrene (PS) and poly(methyl methacrylate) (PMMA) spheres and carbon mixture can be applied as the precursor, through which a thermal treatment can be used to remove the templates. Finally, the foam cathode with a designed porous structure is formed.

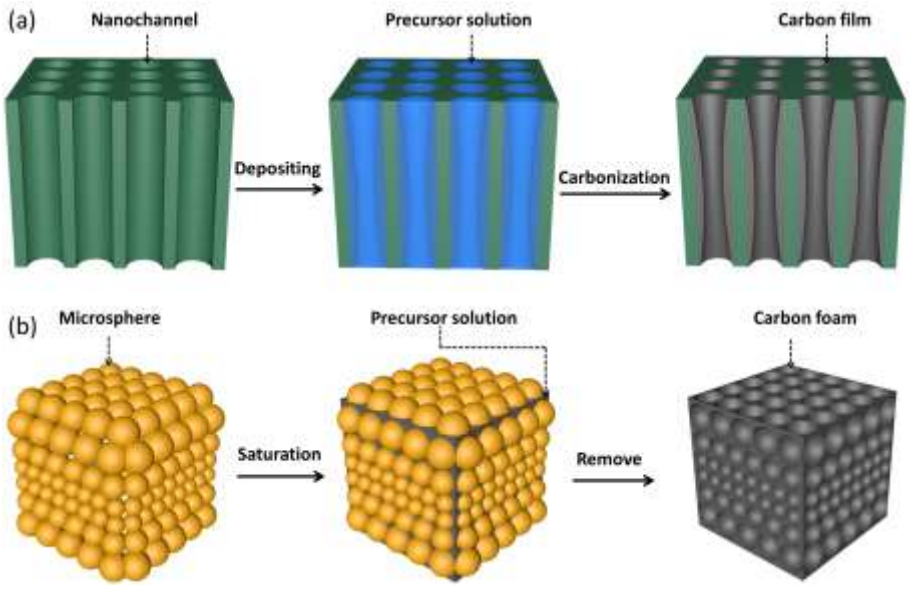

Fig. 8. Scheme of the fabrication process of the cathode with non-uniform porosity (a) ordered AAO template-assisted method and (b) sphere template-assisted method.

5. Conclusions

In this work, we have systematically analyzed the strategies for discharge capacity improvement in aprotic Li-CO_2 batteries. To evaluate the effects of various parameters on the discharge capacity, parameter sensitivity analysis is conducted at different current densities. Based on the results, the initial porosity of the cathode is found to be the most important parameter for capacity improvement and should be carefully designed. To this end, a conventional cathode structure with a uniform porosity is gradually modulated by adjusting into the hierarchical, tapered, parabolic, trapezoid, and frustum conical pore distribution modes. The simulation results demonstrate that a frustum conical porous cathode can deliver the largest capacity improvement of over 60%. Besides, the present sensitivity analysis system is evaluated at high current densities, and the results demonstrate that the limitations

should be overcome by considering the actual capacity and the product morphology. Moreover, the experimental approaches for fabricating the designed cathodes are proposed, including the ordered AAO template and the sphere template-assisted methods. This work highlights the applications and limitations of parameter sensitivity analysis and proposes the design and fabrication of cathode structure for improving the discharge capacity of aprotic Li-CO_2 batteries. In future research, we will mainly concentrate on the simulations of solid product evolution processes as well as experiments of well-designed cathodes for enhanced electrochemical performance.

Acknowledgments

P. Tan thanks the funding support from CAS Pioneer Hundred Talents Program (KJ2090130001), USTC Research Funds of the Double First-Class Initiative (YD2090002006), and USTC Tang Scholar. M. Ni thanks the funding support from The Hong Kong Polytechnic University (G-YW2D) and grants (Project Number: PolyU 152214/17E and PolyU 152064/18E) from Research Grant Council, University Grants Committee, Hong Kong SAR.

Nomenclature

c	concentration (mol m^{-3})
D	diffusion coefficient (m^2 s^{-1})
E	potential (V)
F	Faraday constant (96,485 C mol^{-1})

G change rate of specific capacity

g specific capacity (mAh g^{-1})

I interfacial current density (A m^{-2})

i current density (A m^{-2})

k rate constant; the number of analysis values

L length (m)

M sensitivity index

N molar flux

R reaction rate (mol m^{-3} s^{-1}); electrical resistivity (Ω m); ideal gas constant (8.314J·mol^{-1} K^{-1})

r radius (nm)

T temperature (K)

W molecular weight (g mol^{-1})

X change rate of parameter value

x parameter value

Greek letters

α symmetry factor

ε porosity or volume fraction

η overpotential (V)

κ ionic conductivity (S m^{-1})

φ Li_2CO_3 volume fraction

ρ density (kg m^{-3})

σ electrical conductivity (S m^{-1})

ϕ electric potential (V)

Superscripts and subscripts

0 equilibrium or initial value

app applied value

a anode

c cathode

l liquid electrolyte

n the rank number

s solid electrode or product

References

[1] Liu B, Sun Y, Liu L, Chen J, Yang B, Xu S, et al. Recent advances in understanding Li-CO_2 electrochemistry. Energy Environ Sci 2019;12:887–922.

[2] Xie Z, Zhang X, Zhang Z, Zhou Z. Metal–CO_2 Batteries on the Road: CO_2 from Contamination Gas to Energy Source. Adv Mater 2017;29:1605891–9.

[3] Yang S, He P, Zhou H. Exploring the electrochemical reaction mechanism of carbonate oxidation in Li-air/CO_2 battery through tracing missing oxygen. Energy Environ Sci 2016;9:1650–4.

[4] Yin W, Grimaud A, Lepoivre F, Yang C, Tarascon JM. Chemical vs

Electrochemical Formation of Li_2CO_3 as a Discharge Product in Li-O_2/CO_2 Batteries by Controlling the Superoxide Intermediate. J Phys Chem Lett 2017;8:214–22.

[5] Mu X, Pan H, He P, Zhou H. Li–CO_2 and Na–CO_2 Batteries : Toward Greener and Sustainable Electrical Energy Storage. Adv Mater 2019;1903790:1–22.

[6] Wang T, Sang X, Zheng W, Yang B, Yao S, Lei C, et al. Gas Diffusion Strategy for Inserting Atomic Iron Sites into Graphitized Carbon Supports for Unusually High-Efficient CO_2 Electroreduction and High-Performance Zn–CO_2 Batteries. Adv Mater 2020;2002430:1–9.

[7] Qiao Y, Yi J, Wu S, Liu Y, Yang S, He P, et al. Li-CO_2 electrochemistry: a new strategy for CO_2 fixation and energy storage. Joule 2017;1:359–70.

[8] Mahne N, Renfrew SE, McCloskey BD, Freunberger SA. Electrochemical Oxidation of Lithium Carbonate Generates Singlet Oxygen. Angew Chemie Int Ed 2018;57:5529–33.

[9] Vörös M. A Long-Cycle-Life Lithium–CO_2 Battery with Carbon Neutrality. Adv Mater 2019;31:1902518.

[10] Wu G, Li X, Zhang Z, Dong P, Xu M, Peng H, et al. Design of ultralong-life Li-CO_2 batteries with IrO_2 nanoparticles highly dispersed on nitrogen-doped carbon nanotubes. J Mater Chem A 2020;8:3763–70.

[11] Li C, Guo Z, Yang B, Liu Y, Wang Y, Xia Y. A Rechargeable Li-CO_2 Battery with a Gel Polymer Electrolyte. Angew Chemie - Int Ed 2017;56:9126–30.

[12] Hu X, Li Z, Chen J. Flexible Li-CO_2 Batteries with Liquid-Free Electrolyte. Angew Chemie Int Ed 2017;56:5785–9.

[13] Qiu F, Ren S, Mu X, Liu Y, Zhang X, He P, et al. Towards a stable Li–CO_2 battery: The effects of CO_2 to the Li metal anode. Energy Storage Mater 2019;26: 443-7.

[14] Chih-Jung Chen, Jun-Jie Yang, Chien-Hung Chen, Da-Hua Wei S-FH and R-SL. Improvement of Lithium Anode Deterioration for Ameliorating Cyclabilities of Non-aqueous Li-CO_2 Batteries. Nanoscale 2020;12:8385–96.

[15] Xiao X, Tan P, Zhu X, Dai Y, Cheng C, Ni M. Investigation on the discharge and charge behaviors of Li-CO_2 batteries with carbon nanotube electrodes. ACS Sustain Chem Eng 2020;8:9742–50.

[16] Li J, Wang L, Zhao Y, Li S, Fu X, Wang B, et al. Li-CO_2 Batteries Efficiently Working at Ultra-Low Temperatures. Adv Funct Mater 2020;2001619:1–10.

[17] Xu S, Chen C, Kuang Y, Song J, Gan W, Liu B, et al. Flexible lithium–CO_2 battery with ultrahigh capacity and stable cycling. Energy Environ Sci 2018;11:3231–7.

[18] Xiao Y, Du F, Hu C, Ding Y, Wang ZL, Roy A, et al. High-Performance Li-CO_2 Batteries from Free-Standing, Binder-Free, Bifunctional Three-Dimensional Carbon Catalysts. ACS Energy Lett 2020;5:916–21.

[19] Xu S, Das SK, Archer LA. The Li-CO_2 battery: A novel method for CO_2 capture and utilization. RSC Adv 2013;3:6656–60.

[20] Li Y, Zhou J, Zhang T, Wang T, Li X, Jia Y, et al. Highly Surface-Wrinkled and N-Doped CNTs Anchored on Metal Wire: A Novel Fiber-Shaped Cathode toward High-Performance Flexible Li–CO_2 Batteries. Adv Funct Mater 2019;1808117:1–13.

[21] Khurram A, He M, Gallant BM. Tailoring the Discharge Reaction in Li-CO_2 Batteries through Incorporation of CO_2 Capture Chemistry. Joule 2018;2:2649–66.

[22] Han Y, Liu Y, Dong Y, Wang B, Li S, Hong S, et al. Mono-Dispersed MnO Nanoparticles in Graphene-Interconnected N-Doped 3D Carbon Framework as Highly efficient Gas Cathode in Li-CO_2 Batteries. Energy Environ Sci 2019;12:1046–54.

[23] Zhang X, Zhang Q, Zhang Z, Chen Y, Xie Z, Wei J, et al. Rechargeable Li-CO_2 batteries with carbon nanotubes as air cathodes. Chem Commun 2015;51:14636–9.

[24] Zhang Z, Wang XG, Zhang X, Xie Z, Chen YN, Ma L, et al. Verifying the Rechargeability of Li-CO_2 Batteries on Working Cathodes of Ni Nanoparticles Highly Dispersed on N-Doped Graphene. Adv Sci 2018;5:1700567.

[25] Li J, Zhao H, Qi H, Sun X, Song X, Guo Z, et al. Drawing a Pencil-Trace Cathode for a High-Performance Polymer-Based Li–CO_2 Battery with Redox Mediator. Adv Funct Mater 2019;29:1806863.

[26] Jiang K, Liu X, Lou G, Wen Z, Liu L. Parameter sensitivity analysis and cathode

structure optimization of a non-aqueous Li–O_2 battery model. J Power Sources 2020;451:227821.

[27] Tan P, Shyy W, An L, Wei ZH, Zhao TS. A gradient porous cathode for non-aqueous lithium-air batteries leading to a high capacity. Electrochem Commun 2014;46:111–4.

[28] Gaya C, Yin Y, Torayev A, Mammeri Y, Franco AA. Investigation of bi-porous electrodes for lithium oxygen batteries. Electrochim Acta 2018;279:118–27.

[29] Wang H, Wang H, Huang J, Zhou X, Wu Q, Luo Z, et al. Hierarchical Mesoporous/Macroporous Co-Doped NiO Nanosheet Arrays as Free-Standing Electrode Materials for Rechargeable Li-O_2 Batteries. ACS Appl Mater Interfaces 2019;11:44556–65.

[30] Kang J, Li OL, Saito N. Hierarchical meso-macro structure porous carbon black as electrode materials in Li-air battery. J Power Sources 2014;261:156–61.

[31] Wang F, Li X. Pore-Scale Simulations of Porous Electrodes of Li-O_2 Batteries at Different Saturation Levels. ACS Appl Mater Interfaces 2018;10:26222–32.

[32] Kim DS, Park YJ. A simple method for surface modification of carbon by polydopamine coating for enhanced Li-air batteries. Electrochim Acta 2014;132:297–306.

[33] Xia C, Bender CL, Bergner B, Peppler K, Janek J. An electrolyte partially-wetted cathode improving oxygen diffusion in cathodes of non-aqueous Li-air batteries. Electrochem Commun 2013;26:93–6.

[34] Corrêa JM, Farret FA, Popov VA, Simões MG. Sensitivity analysis of the modeling parameters used in simulation of proton exchange membrane fuel cells. IEEE Trans Energy Convers 2005;20:211–8.

[35] Zhou L, Yan W, Yu Z, He W, Liu M, Liu J, et al. Carbon Nanotube@ RuO_2 as a High Performance Catalyst for Li–CO_2 Batteries. ACS Appl Mater Interfaces 2019;11:5146–51.

[36] Liu L, Guo H, Fu L, Chou S, Thiele S, Wu Y, et al. Critical Advances in Ambient Air Operation of Nonaqueous Rechargeable Li – Air Batteries. Small 2019;1903854:1–32.

[37] Sahapatsombut U, Cheng H, Scott K. Modelling of electrolyte degradation and cycling behaviour in a lithium-air battery. J Power Sources 2013;243:409–18.

[38] Jung CY, Zhao TS, An L. Modeling of lithium-oxygen batteries with the discharge product treated as a discontinuous deposit layer. J Power Sources 2015;273:440–7.

[39] Lee HC, Park JO, Kim M, Kwon HJ, Kim JH, Choi KH, et al. High-Energy-Density Li-O_2 Battery at Cell Scale with Folded Cell Structure. Joule 2019;3:542–56.

[40] Xiao X, Shang W, Yu W, Ma Y, Tan P, Chen B, et al. Toward the rational design of cathode and electrolyte materials for aprotic Li-CO_2 batteries: A numerical investigation. Int J Energy Res 2020;44:496–507.

[41] Lim HK, Lim HD, Park KY, Seo DH, Gwon H, Hong J, et al. Toward a

lithium-"Air" battery: The effect of CO_2 on the chemistry of a lithium-oxygen cell. J Am Chem Soc 2013;135:9733–42.

[42] Laoire CO, Mukerjee S, Abraham KM, Plichta EJ, Hendrickson MA. Influence of Nonaqueous Solvents on the Electrochemistry of Oxygen in the Rechargeable Lithium-Air Battery. J Phys Chem C 2010;114:9178–86.

[43] Read J, Mutolo K, Ervin M, Behl W, Wolfenstine J, Driedger A, et al. Oxygen Transport Properties of Organic Electrolytes and Performance of Lithium/Oxygen Battery. J Electrochem Soc 2003;150:A1351.

[44] Ge B, Sun Y, Guo J, Yan X, Fernandez C, Peng Q. A Co-Doped MnO_2 Catalyst for Li-CO_2 Batteries with Low Overpotential and Ultrahigh Cyclability. Small 2019;1902220:1–8.

[45] Liu W, Shen Y, Yu Y, Lu X, Zhang W, Huang Z, et al. Intrinsically Optimizing Charge Transfer via Tuning Charge/Discharge Mode for Lithium–Oxygen Batteries. Small 2019;15:1–8.

[46] Hu A, Shu C, Xu C, Liang R, Li J, Zheng R, et al. Design strategies toward catalytic materials and cathode structures for emerging Li-CO_2 batteries. J Mater Chem A 2019;7:21605–33.

[47] Mahne N, Fontaine O, Thotiyl MO, Wilkening M, Freunberger SA. Mechanism and performance of lithium-oxygen batteries – a perspective. Chem Sci 2017;8:6716–29.

[48] Scott K. Modelling the microemacro homogeneous cycling behaviour of a

lithiumeair battery. J Power Sources 2013;227:243–53.

[49] Li X, Zhou J, Zhang J, Li M, Bi X, Liu T, et al. Bamboo-Like Nitrogen-Doped Carbon Nanotube Forests as Durable Metal-Free Catalysts for Self-Powered Flexible Li–CO_2 Batteries. Adv Mater 2019;1903852:1–9.

[50] Wei Q, Fu Y, Zhang G, Yang D, Meng G, Sun S. Rational design of novel nanostructured arrays based on porous AAO templates for electrochemical energy storage and conversion. Nano Energy 2019;55:234–59.

[51] Lee KT, Cho J. Roles of nanosize in lithium reactive nanomaterials for lithium ion batteries. Nano Today 2011;6:28–41.

[52] Shen C, Xie J, Liu T, Zhang M, Andrei P, Dong L, et al. Influence of Pore Size on Discharge Capacity in Li-Air Batteries with Hierarchically Macroporous Carbon Nanotube Foams as Cathodes. J Electrochem Soc 2018;165:A2833–9.

[53] Xu JJ, Wang ZL, Xu D, Meng FZ, Zhang XB. 3D ordered macroporous $LaFeO_3$ as efficient electrocatalyst for Li-O_2 batteries with enhanced rate capability and cyclic performance. Energy Environ Sci 2014;7:2213–9.